

## INVESTIGATION OF ELECTROSTATIC PRECIPITATOR CHAR COLLECTOR DESIGNS USING COMPUTATIONAL FLUID DYNAMICS.

Simon VUN<sup>1\*</sup>, Andrew CAMPBELL<sup>1</sup> and John HORROCKS<sup>2</sup>

<sup>1</sup> WorleyParsons Pty Ltd, Melbourne, Victoria 3000, AUSTRALIA

<sup>2</sup> TRUenergy, Yallourn, Victoria 3825, AUSTRALIA

\*Corresponding author, E-mail address: Simon.Vun@worleyparsons.com

### ABSTRACT

WorleyParsons provides Advanced Engineering services through using Computational Fluid Dynamics (CFD) and other numerical methods to analyse improve and minimise the risk of any potential design. This paper provides an overview of the modelling of char collector options for a coal fired power station.

The small cyclone char collectors on the stage 1 Yallourn power station in Victoria are close to the end of their useful life. A parallel flange channel char collector design, installed on the Stage 2 electrostatic precipitators (ESP), was explored as a replacement for the cyclone char collectors. CFD modelling was conducted on the Stage 2 ESP to develop an appropriate design for the Stage 1 char collectors. A particle laden flow was introduced and Lagrangian particle tracking to predict the trajectory of char and ash through the ESP's. The results of the Stage 2 design was used to retrofit a similar design in stage 1 to determine appropriate solutions.

### NOMENCLATURE

<b>F</b>	force
$p$	pressure
<b>U</b>	velocity
$\rho$	density
$\mu$	dynamic viscosity
$\sigma$	stress tensor

### INTRODUCTION

The TRUenergy Yallourn power station currently runs four brown coal fired boilers that produce 1450 MW of electricity. The flue gas from the boiler is cleaned of particles by passing it through electro-static precipitators (ESP). There are two stages of ESP's that consist of two units per stage and each unit contains six ESP's (Figure 1). The Stage 1 char collectors at the front of the ESP's are approaching the end of their serviceable life and are being replaced.

The purpose of the ESP's is to clean the hot exhaust gas from the boilers before the gas exits through the chimney stack. The particle laden gas stream enters the inlet duct of the ESP's and passes through char collectors, which remove the larger, lighter particles that have weak electrical properties. The smaller particles that pass through the char collectors are collected by the electro-statically charged plates located behind the char collectors. The clean gas stream then exits the precipitator through the outlet ducts and out the chimney stack.

The stage 1 char collectors consist of a Flakt paraclone design that uses centrifugal forces to remove the particles from the gas stream. Stage 2 uses a lodge Cottrell configuration, which causes particles to follow a tortuous path through rows of parallel channel. The Stage 1 paraclone char collectors have reached the end of their design life and require replacement.

The intent of TRUenergy is to replace the stage 1 char collectors with a similar configuration to stage 2. Computational fluid dynamics (CFD) modelling with ANSYS CFX11 service pack 1 was used to assess the design of the char collectors and determine the characteristics. Modifications were made to the stage 2 char collector design and implemented in the stage 1 char collector replacement design.

### MODEL DESCRIPTION

#### Governing Equations.

To model the flow of gas and particles an Eulerian-Lagrangian method was used where particles are explicitly tracked. The Eulerian gas phase was treated as and continuous with the governing equations of mass and momentum time averaged.

$$\frac{\partial \rho}{\partial t} + \nabla \cdot (\rho \mathbf{U}) = 0 \quad (1)$$

$$\frac{\partial \rho \mathbf{U}}{\partial t} + \nabla \cdot (\rho \mathbf{U} \otimes \mathbf{U}) = -\nabla p + \nabla \cdot \sigma \quad (2)$$

Heat transfer was considered to account for buoyancy effects on the particles due to temperature gradients and hence changes in gas density. The particles were treated as discrete and travelled with the continuous gas. The particles were fully coupled and considered as discrete dispersed solids that follow Newton's second law according to the equation

$$m_p \frac{d\mathbf{U}_p}{dt} = \mathbf{F}_D + \mathbf{F}_B \quad (3)$$

$\mathbf{F}_D$  is the force due to drag and represented by

$$\mathbf{F}_D = \frac{1}{2} C_D \rho_g A_p |U_s| (U_g - U_p) \quad (4)$$

Where  $U_s$  is the slip velocity between the particle and the gas phase and  $C_D$  is the drag coefficient.

$F_B$  is the force due to buoyancy governed by the difference in density between the gas and particle.

$$F_B = \frac{\pi}{6} d_p^3 (\rho_p - \rho_g) g \quad (5)$$

As this study is concerned with the gas flow through the char collectors at the front of the ESP the electro-static force term in equation 3 was neglected. Full details of the numerical methods can be found in the user manual of ANSYS CFX11.

### Turbulence Model

A turbulence model was used in the simulations to account for the turbulent velocity fluctuations. This was especially important for the flow at the splitters and lipped channels. The turbulence model used in the simulations was the RANS shear stress transport (SST) model which implements a  $k-\omega$  turbulence model at wall regions and a  $k-\epsilon$  turbulence model in the free stream.

### Geometry and Grid Generation

Two different geometries shown in Figure 1 and Figure 2 were used for the Stage 1 and Stage 2 ESP's, respectively. The physical size of both ESP's is over 20m in length and as such the geometries were simplified by assuming symmetry about a 2m section in the Z direction. For the Stage 2 ESP in Figure 1 the gas flow entered the inlet and passed through 12 splitter plates before entering the char collectors. A curtain was placed behind the char collectors that extended into the hopper below. A set of tapered baffles were placed before the outlet that was designed to increase flow from the top of the ESP. The Stage 1 geometry in Figure 2 has an inlet flow straight onto the char collectors. The ESP plates and the electrostatic charge were omitted for both ESPs as they were outside the scope of this project. In addition the geometry assumed gas could only enter through the inlet and leave via the outlet, which neglected any gas excess or leakage in the system.

The char collectors currently installed in the Stage 2 are made up of three staggered rows of parallel flange channel shown in Figure 3.

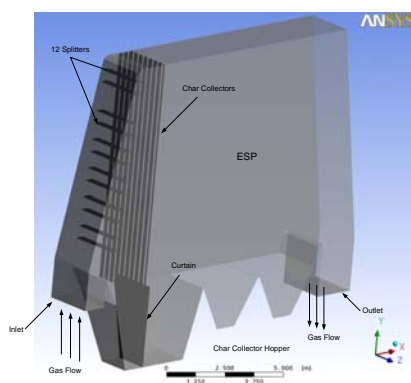


**Figure 1** Geometry of the Stage 2 ESP with three staggered rows of char collector.

### Meshing

The mesh was generated by resolving the flow around the lipped channels on a smaller section of geometry. An analysis was performed on a small test case of the three lipped channel to reduce the amount of nodes required and therefore reduce the computational time.

It was determined however that further refinement was required around the splitters and the lipped channel to reduce the solution residuals in these areas. It was found that 3 million to 7 million nodes were required for the Stage 2 and Stage 1 ESP's without affecting the overall accuracy of the solution. The more rows of channel would substantially increase the number of nodes required.

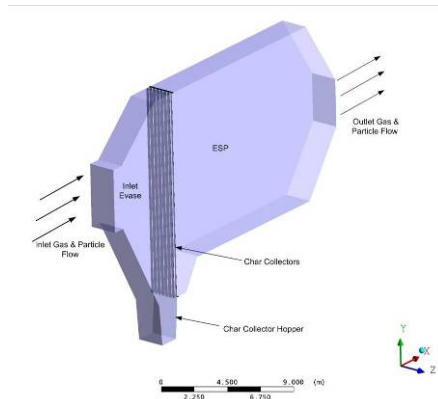


**Figure 2** Geometry of the Stage 1 ESP with three staggered rows of char collector.

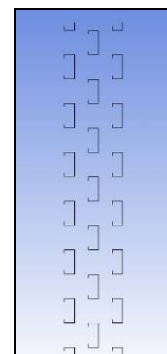


**Figure 3** Lipped channels that form the char collectors, showing the three staggered row arrangement.

### SIMULATION CONDITIONS

The simulations of the flow of gas and particles in the char collector were performed using the commercial CFD software package ANSYS CFX 11 with service pack 1 applied. Steady state simulations were performed with the gas assumed to be incompressible air with discrete sized particles injected at the inlet. The properties of the air and particles are listed in Table 1. Heat transfer and buoyancy were also included to account for any thermal gradient and density difference between the gas and particles.

A Lagrangian particle tracking method used to determine the dispersion of particles through the char collectors. The maximum time the particles were tracked was 20 seconds, for a maximum distance of 40 meters. In the absence of particle size data the diameters in were estimated from paracelone char collector data, provided by TruEnergy of 99% above 246 micron to 75% above 38-43 micron. Previous studies (Kuan, 2007) into char collection investigated particles between 100 and 300 micron.

Properties	Air	Particles
Density (kg/m <sup>3</sup> )	1.185	285
Viscosity (Pa.s)	1.831e-05	-
Heat Capacity (J/kgK)	1004.4	1046
Thermal Conductivity (W/mK)	0.0261	0.2092

**Table 1** Properties of gas and solids.

Based on this data the particle sizes included in the simulations are 10, 40, 150, 250 and 300 micron with a 20% distribution for each size.

**Boundary Conditions**

The inlet conditions assumed a uniform velocity profile and neglected the upstream conditions. The inlet conditions for the gas and particles are listed in Table 2. A uniform inlet profile was used as the data on the upstream conditions was unavailable.

The outlet assumed an opening pressure of zero relative to atmospheric conditions. With heat transfer model included in the simulations the walls of the model were treated as an adiabatic condition.

Parameter	Stage 2	Stage 1
Gas Velocity (m/s)	14.4	11.43
Inlet Particle Mass Flow Rate (kg/s)	0.132	0.669
Inlet Dust Loading (kg/m <sup>3</sup> )	3.89	3.89
Static Temperature (°C)	200	219
Duct Inlet Area (m <sup>2</sup> )	2.369	9.240
Number of Particles	20,000	20,000

**Table 2** Boundary conditions used in the simulations.

A coefficient of restitution was applied to the walls to account for the particle-wall collisions. The coefficient of restitution determines the elasticity of a collision and is 1 for a perfectly elastic collision. The perpendicular and parallel coefficients of restitution used in the simulations were taken from experiments for coal particles impacting steel (Schade, 2002). A 0.36 perpendicular coefficient of restitution and 0.7 parallel coefficient of restitution were applied at the walls. It was noted that expressions for coefficient of restitution as a function of velocity and angle have been developed (Kuan et al, 2007), however they were not used here.

**RESULTS**

To design the Stage 1 char collectors the three stage char collectors were studied in the Stage 2 ESP.

**Stage 2 ESP**

The velocity contour plot in Figure 4 characterizes the cross sectional flow through the Stage 2 ESP. Gas from the inlet passes through splitter plates and enters the char collectors. The particle laden gas then passes through the char collectors and enters the ESP section before leaving through the outlet.

The inlet gas has high vertical velocity, which was distributed across the char collectors by the splitter plates. The 12 splitter plates above the inlet turn the flow 90 degrees onto the char collectors causing recirculation

regions behind the splitter plates. These recirculation regions between the splitter plates and the front of the char collectors are apparent in Figure 5 and Figure 6. The largest recirculation region is shown in Figure 5 and extends from underneath the bottom splitter plate into the char collector hopper. Smaller recirculation regions shown in Figure 6 exist at the top of the inlet housing with the direction of circulation marked.

The particle flows in Figure 7 show the distribution of five particle diameters through the char collector. The overall number of particles introduced through the inlet was 20,000 with 500 particles plotted. Figure 7 shows the larger diameter particles such as 150micron to 300 micron drop out due to the char collectors while the smaller particles of 10 micron to 40 micron tend to pass through the char collectors.

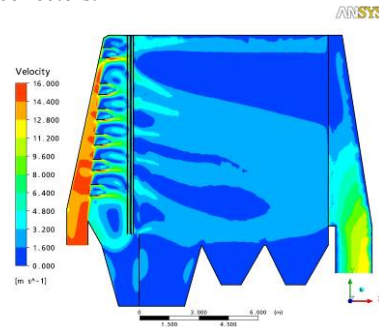


**Figure 4** Gas velocity through cross section of the char collector and ESP. Inlet on the left and outlet on the right.

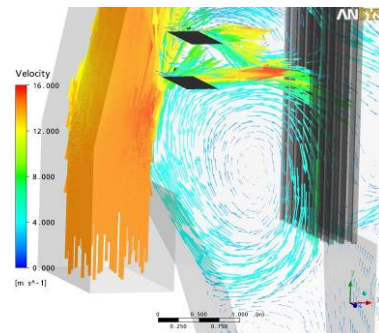


**Figure 5** Cross section of gas recirculation region in front of the char collector, bottom section.

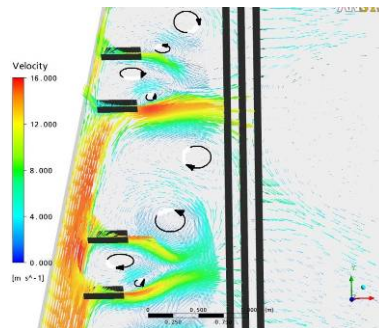


**Figure 6** Cross section of gas recirculation region in front of the char collector top section. Arrows showing direction of circulation.

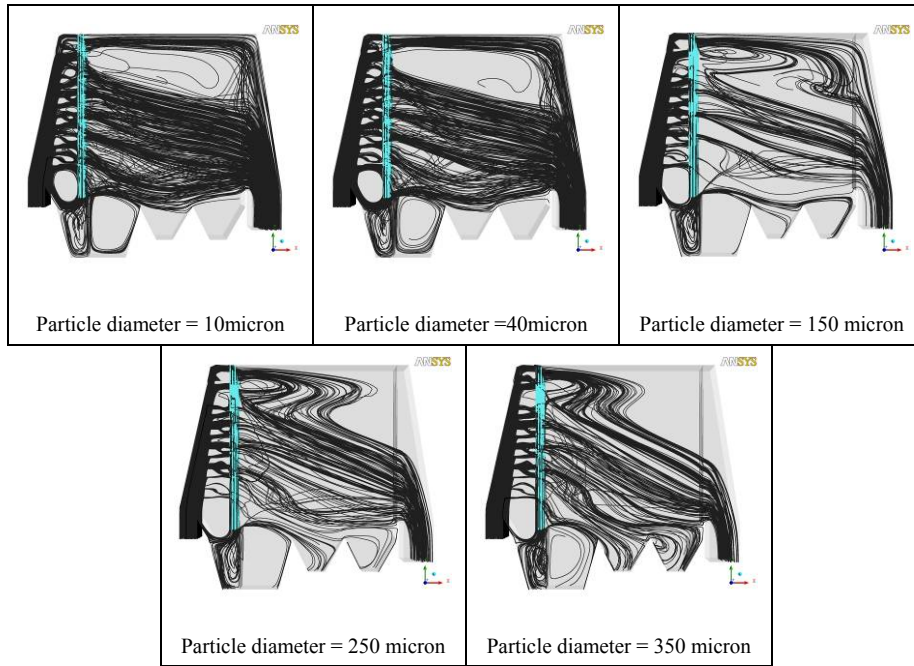


**Figure 7** Particle paths through the Case 1 char collectors for the discrete particle diameters.

	Three row char collector	Six row char collector
<b>Pressure Drop Across Collectors</b>	17 Pa	32 Pa
<b>Pressure Drop Across System</b>	72 Pa	82 Pa

**Table 3** Comparison of pressure drop across the Stage 2 three row and six row char collectors.

The velocity of the gas jet was more profound in simulations of the six staggered row char collector arrangement shown in Figure 8. In addition the difference in pressure drop across the three and six staggered row arrangements is listed in Table 3.

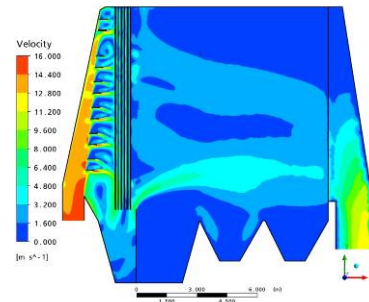


**Figure 8** Gas velocity through cross section of the Stage 2 ESP.

**Stage 1 ESP**

The Stage 1 design was taken from the three staggered row arrangement in the Stage 2 ESPs based on the pressure drop and the particle flow results. The three rows were positioned towards the rear of the hopper to prevent the by-passing of particle laden gas flow through the gap between the char collectors and the hopper.

The gas velocity contour plot through the cross section of the ESP is presented in Figure 9. The velocity contours show the flow from the inlet impacting the front of the collectors, which turn the gas flow 90 degrees vertically in both directions. This resulted in a large recirculation region at the bottom of the inlet evase (Figure 10) and a smaller recirculation region at the top of the inlet evase (Figure 11). The influence of the flow through the char collectors was high flow regions at the top and bottom of the ESP. The pressure drop across the char collectors is listed in Table 4 and on comparison with Table 3 shows a higher pressure drop.

The particle tracks in Figure 12 show the travel path of 500 particles for each of the five particles sizes simulated.

	Three row char collector
<b>Pressure Drop Across Collectors</b>	108 Pa
<b>Pressure Drop Across System</b>	178 Pa

**Table 4** Comparison of pressure drop across the Stage 2 three row and six row char collectors

The majority of smaller sized particles passed through the char collectors. The larger particles drop out due to the impact with the char collectors. However the larger particles tend to be entrained by the high flow regions at the top and bottom of the ESP.

For comparison three configurations of the six staggered row configuration were modelled. The gas flow at the bottom of the char collectors is shown in Figure 13. Similar to Stage 2 the six row char collector produced a jet at the back of the hopper. In addition the velocity streamlines in Figure 13 show the flow at the front short cuts the char collectors and causes the undesirable jet at the rear of the hopper. While six staggered rows with the

curtain in the hopper show an improvement, high velocities at the bottom of the char collectors entrain the larger particles. Both the Stage 1 and Stage 2 six staggered row char collectors have a higher pressure drop than the three staggered row char collectors.

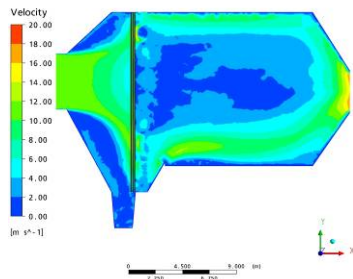


**Figure 9** Gas velocity through cross section of the Stage 1 ESP.

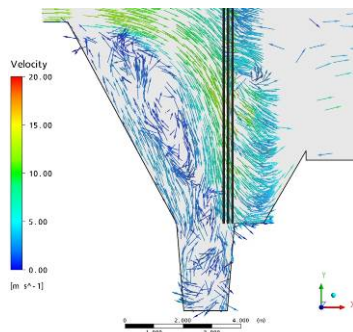


**Figure 10** Cross section of the gas recirculation region at the bottom of the Case 4 char collector.

## DISCUSSION

A combination of the recirculation regions and pressure drop influenced the entrainment of particles into the ESP. In both ESPs a recirculation region existed at the bottom of the char collectors. Simulations showed the recirculation regions penetrated into the char collectors, contributing to entrainment of the larger particles into the ESP. A solution provided for Stage 2 ESPs was the installation of a splitter below the lowest splitter to disrupt the flow within the recirculation region. It is expected with the introduction of the char collectors in the Stage 1 ESPs a screen would be installed after the inlet to distribute the flow across the char collectors.

It was found that the particle capture efficiency would increase when modifications were made to improve the gas flow through the char collectors. Characteristics of the gas flow that would 'short cut' the char collectors usually entrained the particles that were destined for the char collector hopper.

A limitation of the particle behaviour was the lack of information on the particle size distribution and the coefficient of restitution for char.

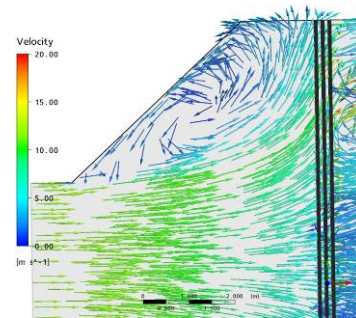


**Figure 11** Cross section of gas recirculation region in front of the char collector top section for Case 4.

Both require experiments of the specific material to determine the required values. While the coefficient of restitution accounted for perpendicular and parallel angles, some particles would oscillate on the surfaces of the char collector without dropping out.

## CONCLUSION

The Stage 1 and Stage 2 ESPs were modelled to study the effectiveness of the staggered row char collectors made up parallel flange channel. The staggered row char collectors from the Stage 2 ESPs were studied with the intent to replace the Stage 1 paraclone char collectors. The Stage 2 three staggered row char collector produced a lower pressure drop than the six row char collector. The advantages of the three staggered row char collector were consistent in the Stage 1 ESP.

## REFERENCES

- SCHADE K.-P., ERDMANN H.-J., HADRICH TH., SCHNEIDER H., FRANK TH, BERNERT K.. (2002), "Experimental and numerical investigation of particle erosion caused by pulverised fuel in channels and pipework of coal-fired power plant", *Powder Tech*, v 125 p242-250.
- KUAN B., REA, N. and SCHWARZ, P. (2007) "Application of CFD in the design of a grit collection system for the coal-fired power generation industry.", *Powder Tech*. v 179 p65-72.

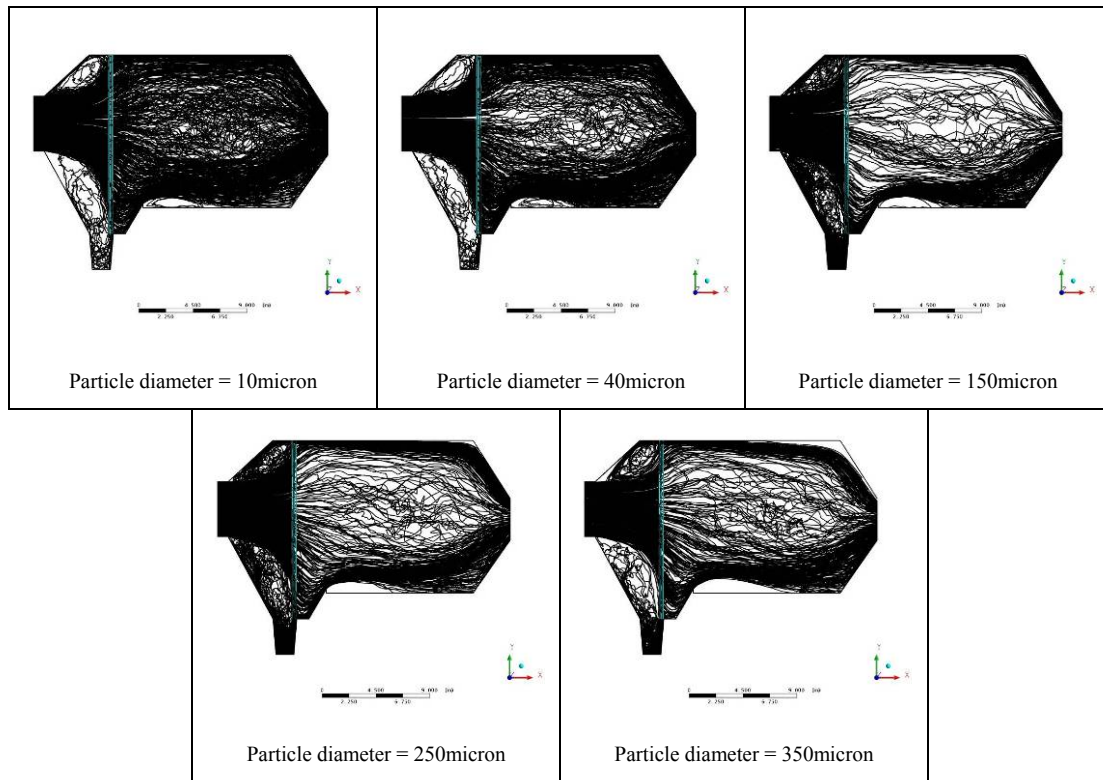


**Figure 12** Particle paths through the Case 4 char collectors for the discrete particle diameters.

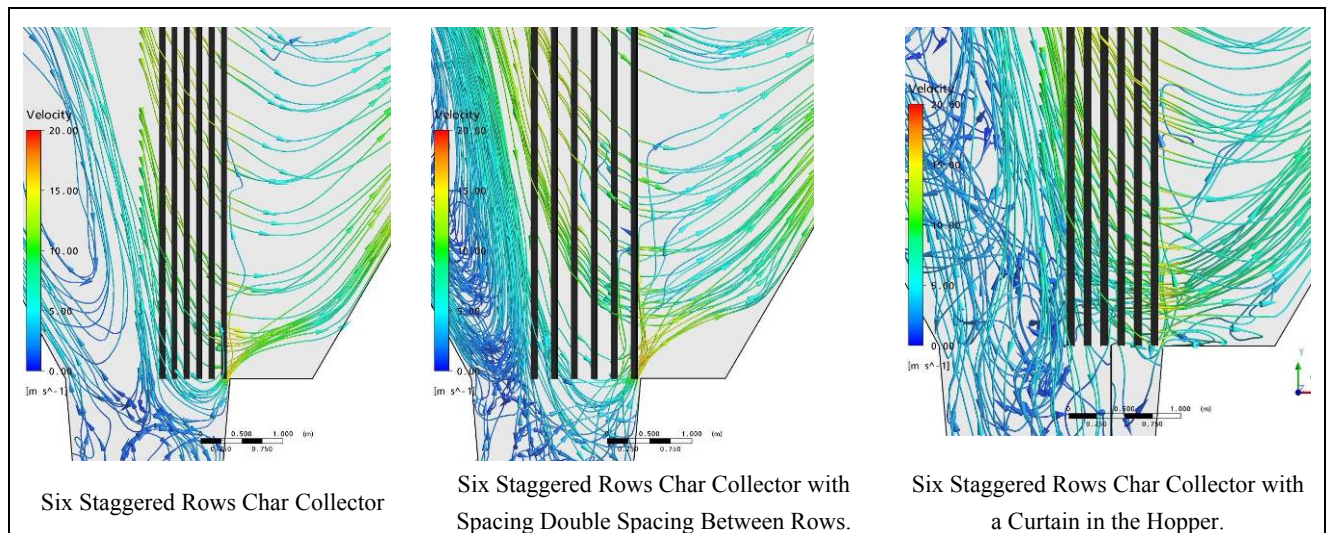


**Figure 13.** The gas flow near the bottom bypasses the last three rows of char collector and forms a high velocity jet between the last row of the char collectors and the hopper wall.